ENVIRONMENTAL RESEARCH
LETTERS

OPEN ACCESS

RECEIVED
19 January 2026

REVISED
13 April 2026

ACCEPTED FOR PUBLICATION
13 May 2026

PUBLISHED
4 June 2026

LETTER

Increase in European summer heatwaves driven by greenhouse gases and amplified by aerosol emission reductions

Tilda Huntingford[1], **Kunhui Ye**[1,*] **and Scott Osprey**[1,2]

[1] Atmospheric, Oceanic and Planetary Physics, University of Oxford, Oxford, United Kingdom
[2] National Centre for Atmospheric Science, Leeds, United Kingdom
[*] Author to whom any correspondence should be addressed.

E-mail: kunhui.ye@physics.ox.ac.uk

Keywords: heatwaves, attribution, external forcings, large-ensembles, climate modelling, atmospheric circulation

Supplementary material for this article is available online

Abstract

More frequent heatwaves in Europe are posing considerable risks to human health, infrastructure, and ecosystems. However, the contributions of external forcing factors such as well-mixed greenhouse gases (GHGs) and aerosols remain to be better quantified. Here, using model outputs from the Large Ensemble Single Forcing Model Intercomparison Project (LESFMIP), a recent atmospheric reanalysis and a machine learning method—self-organising maps (SOMs), we attribute European heatwave trends during 1940–2020 to various external forcings. The Europe-averaged heatwave trend during 1940–2020 (0.87 days per decade) is well captured by the multi-model mean (MMM) response with GHGs dominating the trend. The positive heatwave trend in GHGs and ozone is offset by the effects of aerosols during 1940–1979, leading to weak negative heatwave trends. In contrast, the increase in GHGs has driven about half ($53 \pm 17\%$; MMM and model-spread) of the strong heatwave trends in 1980–2020 (2.5 days per decade), amplified by the reduction in aerosols ($23 \pm 15\%$). This highlights the increasing risk of more frequent heatwaves in Europe if GHG emissions continue to rise without significant mitigation measures. Analysis of atmospheric circulation by SOMs reveals that four major atmospheric circulation patterns, dominated by a blocking high anomaly, are linked to the most spatially-intense European summer heatwaves. A relatively large increase in the occurrence of blocking-like atmospheric circulation has likely exacerbated heatwave trends in Southern and Eastern Europe in 1980–2020. However, this atmospheric circulation trend is much weaker in the model response, and also seems to be outside the internal variability in most of the models. This may partly explain the underestimated heatwave trends in Southern and Eastern Europe. Constraining and further understanding of the thermodynamic and dynamic response in the LESFMIP models is important for attributing and predicting the multi-annual and decadal variability of climate and weather extremes.

1. Introduction

Heatwaves have severe consequences for human health [1, 2], agriculture, increasing risk of crop losses [3], ecosystems [4] and infrastructure. For instance, heightened electricity demand coupled with reduced power production during heatwaves can lead to grid overload [5]. The impact on human health includes increased mortality, exemplified by the over 70 000 deaths attributed to the 2003 Western European heatwave [6] and an estimated 61 672 heat-related deaths in Europe in 2022 [7], as well as heightened respiratory disease risk in urban areas [8]. These health risks can be mitigated through improved early-warning systems [1, 9], which rely on a comprehensive understanding of heatwave drivers to enhance prediction and projection capabilities [10].

The frequency of heatwaves has been increasing since 1950 [11, 12] and their frequency, intensity and spatial extent are expected to rise further throughout the 21st century [13, 14], particularly in mid-latitude regions such as Europe [15, 16]. Changes in heatwaves are driven by both thermodynamic and dynamic factors. Thermodynamic factors

include radiative forcing (changes in Earth's energy balance) and land-atmosphere interactions, including soil moisture [17–19]. Dynamic factors involve atmospheric circulation patterns that increase the persistence and probability of hot events in summer, such as an increased frequency of hemispheric teleconnections [20, 21]. Trends in atmospheric circulation have driven a large fraction of the increase in heat extremes in Western Europe [16, 18, 22] but this has been underestimated by climate models [16, 23], due to their failure to capture forced response or internal variability or both. Additionally, land surface feedback has been considered as a driver of heatwave increase in Europe [24]. These highlight the uncertainties and complexities in understanding the drivers of and in attributing heatwaves in Europe.

Existing attribution studies of European heatwaves indicate that changes in these processes are, at least in part, a response to anthropogenic forcings [25–27], including rising concentrations of well-mixed greenhouse gases (GHGs) [11] and declining aerosol emissions due to air pollution legislation [28]. Aerosols provide negative forcing due to their influence on radiation and clouds but their concentrations over Europe have been declining since the 1980s [29, 30]. The significance of aerosols has been emphasised in recent literature as a driver of weather extremes [31, 32] and summer European warming in particular [33]. Additional contributing factors may include volcanic activity, ozone variability, natural forcings, land use, internal climate variability and the Atlantic Multidecadal Oscillation. However, the full range of physical processes and drivers underlying observed heatwave trends remains incompletely understood and quantified.

In this study, we use climate simulations from seven state-of-the-art coupled climate models, contributing to the Large Ensemble Single Forcing Model Intercomparison Project (LESFMIP) [34] and a recent atmospheric reanalysis to attribute the recent trends in summer heatwave frequency (HWF) in Europe. The large-ensemble single forcing climate simulations allow us to robustly quantify the contributions of various external forcing factors, while the use of multiple models accounts for model uncertainty. Small ensemble climate simulations in some previous attribution studies [27, 35, 36] are not optimal for quantifying the roles of forced versus internal variability in driving heat extremes. In addition, we use an unsupervised machine learning method—self-organising maps (SOMs) to identify the main atmospheric circulation patterns that are linked to European summer heatwaves. Our attribution analysis thus provides novel and quantitative insights into the drivers of recent increases in European summer heatwaves, including atmospheric circulation trends.

2. Data and methods

2.1. Atmospheric reanalysis data

Europe is defined as the domain of 36°–72° N and 25° W–45° E. The variables used in this study were daily maximum temperature at 2 m (TX) and daily mean geopotential height at 500 hPa (Z500). We use the fifth generation of atmospheric reanalysis of the global climate produced by the European Centre for Medium-Range Weather Forecasts (ERA5) [37] with a temporal coverage of 1940 to 2025 and a spatial resolution of 0.25 degrees. ERA5 reliably captures extreme temperatures in Europe [38, 39].

2.2. Attribution of European heatwave trends using the LESFMIP model experiments

Coupled model experiments from the LESFMIP project provide a new capability for attributing multi-annual and decadal changes in the climate system [34]. Specifically, these multi-model large-ensemble initial-condition climate simulations imposed with historical external forcings allow for robustly isolating the contributions of individual external forcings in the changes in the climate system. This addresses both internal climate variability and model uncertainty for attribution of multi-annual and decadal changes. We note that potential model errors, signal-to-noise paradox, imperfect historical forcings and missing processes may contribute to uncertainties in these LESFMIP model experiments [34]. In this study, we focus on the multi-model mean (MMM), defined as the unweighted average across individual model's ensemble average, and direct trend-comparison approach for attributing European heatwave trends. This approach is less robust to model errors and does not consider the optimal linear combination of individual forcings, compared to the multiple linear regression framework [40].

We obtain available outputs from seven models: ACCESS-ESM1-5 [41], CanESM5 [42], CMCC-CM2-SR5 [43], HadGEM3-GC31-LL [44], MIROC6 [45], MPI-ESM1-2-LR [46] and NorESM2-LM [47]. The experiments used in our study include the all-forcings 'historical' experiment and six historical single-forcing experiments with specified historical evolutions of the relevant forcings. These are hist-GHG (historical variations in well-mixed GHGs), hist-aer (historical variations in anthropogenic aerosols), hist-sol (solar irradiance variability), hist-volc (volcanic stratospheric aerosols), hist-nat (historical variations in natural influences–solar and volcanic) and hist-totalO3 (ozone concentration) [34]. The hist-lu (land use changes) experiment was not considered in this study due to insufficient available data. Details of these experiment including the number of ensemble members are given in supplementary tables

1 and 2. We extended the all-forcing historical experiment for TX to 2020 using the future scenario (SSP2-4.5) experiment for the period 2015–2020 [48].

A comparison of the summer (June-August, JJA) climatology of TX for 1981–2010 from ERA5 with the climatology of each LESFMIP model suggests a close agreement (supplementary figure 1), supporting the suitability of the LESFMIP models to study European heatwaves.

2.3. Heatwave frequency

This study focuses on daytime heatwaves occurring during the meteorological summer (JJA). The heatwave threshold is defined as the 90th percentile of TX based on a 15-day window for each calendar day [49, 50], over the period 1940–2014; limited by the data availability for some models. A heatwave is defined as a period of at least three consecutive days during which the TX at a given grid point exceeds its heatwave threshold. While a combination of high daily maximum and minimum temperatures and humidity have the largest impacts on human health [1], an analysis using only TX, capturing mainly daytime heatwaves, was deemed satisfactory to identify key heatwave trends for this study [14, 49]. We adopt the common use of HWF, defined as the number of days that contribute to heatwaves for each grid point for each summer [10, 49]. In this study, 'HWF trends' is interchangeable with 'heatwave trends', as other heatwave metrics are not considered. To consider spatially-concurring heatwave events extending across multiple grid points, we consider European heatwave events as described in the next sub-section.

2.4. European heatwave days

European heatwave days are defined as those JJA days with the largest land area covered by heatwaves on a given day. This is calculated by computing the percentage of land grid points (weighted by area) experiencing a heatwave on any JJA day in the predefined European domain. Then, the top 10% of days are selected as European heatwave days. This retains large-scale, high-impact heatwave events in Europe while still ensuring a sufficient number of heatwave events for further analysis.

2.5. Linear trends, statistical significance and computation of area-mean

To quantify long-term trends in European summer heatwaves, linear trends are calculated using non-parametric Theil–Sen regression, which is robust against outliers and does not assume a normal distribution. This will ensure that the trend obtained is not distorted by some extreme values in a time series and is not distribution-dependent. The statistical significance of these trends is assessed using the Mann–Kendall test at the 5% level. For the SOMs analysis as described below, there are many zero entries for the number of days assigned to each node due to the nature of the classification. Given that the Theil–Sen method calculates the median slope, it was not suitable for the original time series of heatwave days, as it leads to an overall zero trend. Therefore, the trends on circulation occurrence are computed after applying a 5-year running average.

For model outputs, trends are calculated for each ensemble member before taking an ensemble average. Uncertainty in the MMM is calculated using bootstrapping, resampling members inside each model independently before averaging across models to show confidence intervals (CIs). Model spread is quantified using standard deviation (STD) over individual model means.

Spatial averages are computed with weights of $cos(latitude)$ and sea areas are masked. The ERA5 land sea mask is also applied to model outputs, which are regridded to an ERA5 grid for this purpose. Spatially averaged trends are calculated by first performing spatial averaging of the time series and then calculating the trend. The alternative approach, reordering the steps, gave similar results. Where spatial averages are cited for Southern or Northern Europe, the dividing latitude is taken to be 50 ° N.

2.6. Self-organising maps

SOMs are a type of artificial neural network used for unsupervised machine learning, enabling the classification of data into a specified number of nodes. SOMs have become a widely used tool for classifying large-scale atmospheric circulation patterns during extreme events [20, 51, 52]. We use daily Z500 anomalies, relative to the 1980–2010 climatology, to characterise large-scale atmospheric flow patterns linked to European heatwaves. The data was weighted by $\sqrt{\cos(\text{latitude})}$, to prevent biases toward regions with higher grid resolution [53]. The SOMs were trained only on European heatwave days (see section 2.4) from 1940 to 2014, and over the domain of 20 °–90 ° N and 90 ° W–90 ° E.

Following Lee *et al* [20], the number of SOM nodes must be chosen to (a) be large enough to accurately capture the patterns in the data, and (b) small enough so that each pattern is distinct. We quantify (a) by computing the weighted mean pattern correlation: the pattern correlations between the daily Z500 patterns and their assigned SOM pattern, averaged over all SOM nodes and weighted by the corresponding SOM frequency [54]. We quantify (b) by calculating the average of the weighted Euclidean distance d between different pairs of nodes [20]. By comparing 1D grids between (2 × 1) and (10 × 1), we found that a (4 × 1) SOM grid best satisfied the requirements to maximise the weighted mean pattern correlation (WMPC), while ensuring the nodes remained distinct.

To quantify the role of GHGs and aerosols on European HWF trends, we computed SOMs for

ERA5, and three model experiments, namely all-forcings, hist-GHG and hist-aer. Fewer models had available data for Z500 than for TX. For model outputs, the training data is from the pooled European heatwave days from all ensemble members and four spatial patterns of Z500 are obtained for each model experiment. A cost matrix was then used to match model nodes to each ERA5 node, where a spatial pattern correlation of less than 0.4 is considered to have no clear counterpart in that model experiment. The WMPC for the ERA5 SOM was 0.46 and so 0.4 was deemed a reasonable pattern correlation threshold for comparison with the other nodes for each model experiment, but other thresholds (including no threshold) were also tested with limited effects on the results.

2.7. Trends in the SOM atmospheric circulation patterns based on all JJA days

To assess whether the SOM nodes themselves are increasing in frequency, we project the circulation patterns for all JJA days onto the four ERA5 nodes. This was done using Pearson pattern correlations between the four ERA5 SOM nodes and the daily Z500 patterns for all JJA days for each model experiment. An alternative method using Euclidean distance to compare the patterns was also tested, giving similar results. The threshold of 0.4 was chosen for the same reason as above, and days with a pattern correlation of less than 0.4 with all nodes were left unassigned. Thresholds between 0.2 and 0.7 were also tested (supplementary figure 2), showing that results were not sensitive to threshold. Applying this threshold value led to the presence of zero values over some years in the obtained time series. This is expected as a similar circulation pattern linked to the most spatially-expansive heatwaves does not necessarily appear in all the years. The Theil–Sen method, which calculates trends using the median slope, would suggest no trends. As discussed in section 2.5, we applied a 5-year running average to the time series before computing trends. The projection procedure also allowed us to calculate the percentage of heatwaves at each gridpoint assigned to each node (supplementary figure 3), giving spatial maps of which node is relevant for heatwaves in different regions.

3. Results

3.1. Historical European summer HWF trends

The European-average HWF is observed to increase significantly from around 1980 (red, figure 1(a)), consistent with the upward trend in the daily maximum temperature (blue, figure 1(a)). The HWF value for 2025 was roughly 4 times as large as it was in 1980. In contrast, it shows virtually no trend before 1980. This drastic increase in European HWF has been reported in many previous studies [14, 27, 55, 56]. To further understand the recent upward trend in HWF, spatial trends of HWF for ERA5 data for pre-1980 and post-1980 are given in figures 1(b) and (c). They clearly confirm the rapid increase in HWF in most of Europe after 1980, and particularly over Southern and Eastern Europe (figure 1(c)). The area-averaged post-1980 HWF trend for Southern Europe (south of 50° N) is 2.8 days per decade. The MMM simulations with all historical forcings reproduce these drastic trends after 1980, similarly highlighting the largest trends in Southern Europe (figure 1(e)). The MMM still underestimates the HWF trends in ERA5 as is noted in some previous studies [16, 33] particularly in Eastern Europe. This is also true for individual models (supplementary figure 4).

The overall consistency in terms of temporal trends and spatial pattern between ERA5 and the MMM suggests that external forcings play an important role in driving the rapid increase in HWF over Europe after 1980. However, existing studies have not systematically attributed these trends to individual external forcings, though the effects of increasing GHGs have been widely proposed [57, 58]. Heatwaves are increasingly linked to mortality in Europe and a better attribution of heatwave change is clearly beneficial; [59] provides a comprehensive dataset of 854 European cities for 2000–2020 and heat-related standardised excess death rates (per 100 000 person-years). Heat-related deaths show a similar spatial pattern to HWF (figure 1), showing the strong link between the increase in heatwaves, and their societal and health impacts. Similar spatial patterns of mortality are found for specific recent summers in [7, 60].

3.2. Attribution of European summer HWF trends to external forcings

As seen in the upper panel of figure 2, European-average HWF is mostly consistent between ERA5 (black) and the MMM with all historical forcings (blue), both showing rapid upward trends in recent decades. The time series for the GHG MMM (blue) has a consistent positive trend throughout the whole period, while aerosols (red) show a negative trend prior to 1980 and a positive trend afterwards. All other single forcing experiments show limited trends. To attribute the HWF trends to external forcings and quantify their effects, we compare individual trends for single-forcings and historical all-forcings to ERA5 for three time periods (lower panel, figure 2).

We first focus on the post-1980 period as it has a rapid HWF trend in Europe, with a trend of around 2.5 days per decade in ERA5 (black cross). The MMM with all historical forcings (black dashed) well captures this trend. While there are a wide range of trend values for individual models (1.7–3.3 days per decade), the bootstrapping method (section 2.5) shows that this MMM is robust (grey shading). Around 53% (95% CI = 49%–58%, STD = 17%) of the HWF trend in the MMM with historical forcings is attributed to

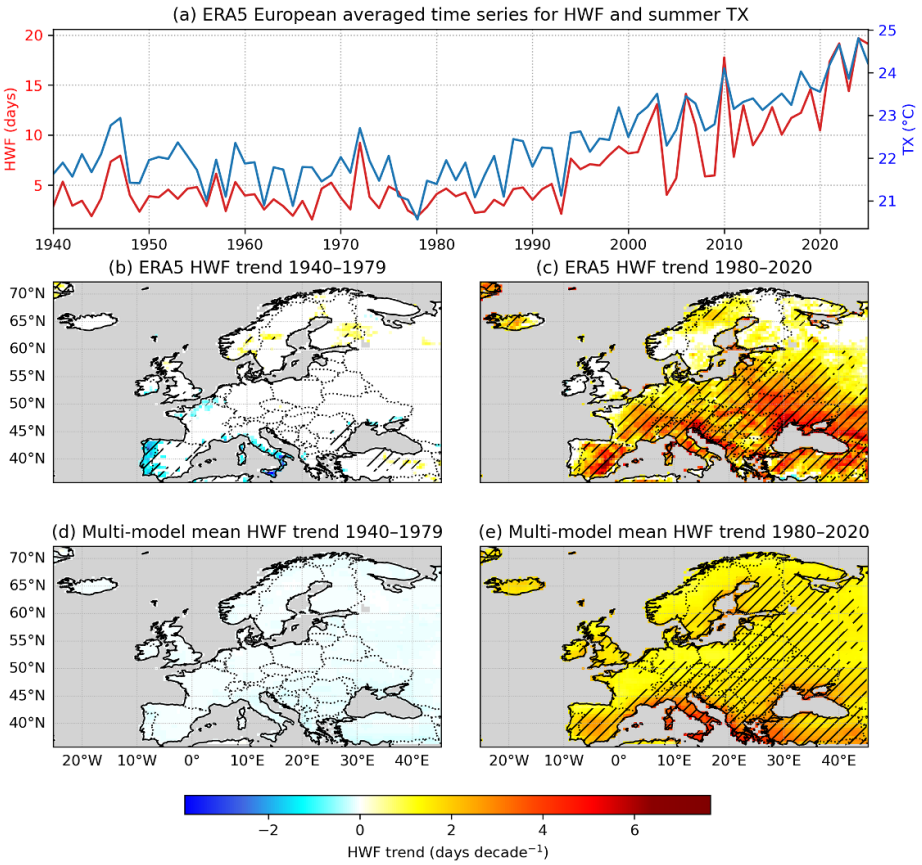

Figure 1. Heatwave frequency in Europe and its spatial trends. (a) Time series of HWF and summer TX averaged over Europe's land from 1940 to 2025 for ERA5. (b)–(e) Spatial patterns of trends in HWF for two periods, 1940–1979 and 1980–2020, in day decade^{-1} for ERA5 (b), (c) and for the MMM (d), (e). Hatching indicates trends which are significant at the 5% level or, for the model, where at least 50% of the models show significance.

GHGs, and 23% (95% CI = 20%–26%, STD = 15%) attributed to aerosols. The contributions from other external forcings are small, with volcanic forcing contributing 12% (95% CI = 9%–15%, STD = 2.7%). We suggest that the recent European HWF trend is mainly attributed to rising GHGs and is amplified by a reduction in aerosols [28]. For this period, the total contribution by linearly adding individual contributions explains about 88% (95% CI = 72%–104%) of the ERA5 HWF trend smaller than that by the historical forcing. This suggests there may be some nonlinear interactions between different forcings. Again, we note that the inter-model spread is considerable for both GHGs and aerosol effects. This highlights the need to sample model uncertainties and the advantage of the multi-model large-ensemble approach used in our study.

The ERA5 HWF trend is negligible for 1940–1979 (black). The MMM trend with all historical forcings (blue) is also weakly negative, and the MMM trends with GHGs (green) and O3 (light grey) are weakly positive. However, the MMM trend with aerosols (red) is largely negative, with considerable inter-model spread. This suggests a highly variable response to aerosols forcing between models. The MMM trends for other external forcings are rather small. A linear addition of all individual forcings would give a large negative HWF trend, dominated by aerosols, of much greater magnitude than that found in the historical forcing experiment. GHGs and O3 may have offset aerosols effects via nonlinear interactions to induce the small HWF trend in the 1940–1979 historical forcing experiment. Nonlinear interactions include aerosol-temperature feedback, where increases in GHGs reduce aerosol burden [61]. However, this nonlinear interaction is not represented in the model experiments analysed in this study since historical external forcings are prescribed.

When considering the entire period, 1940–2020, external forcings explain most of the ERA5 HWF trend (of 0.87 days per decade). GHGs are the main driver of the trend, weakly compensated by aerosols, and with other external forcings playing a negligible role. This is expected given the dominant role of GHGs in driving the significant HWF trend in the recent period (1980–2020). Natural forcings have a limited effect on long-term European summer heatwave trends in our study and instead act as short-term perturbations [62]. In the remainder of the study, we will focus on understanding the atmospheric circulation linked to the European HWF trend in the latter period 1980–2020. Given the continuous

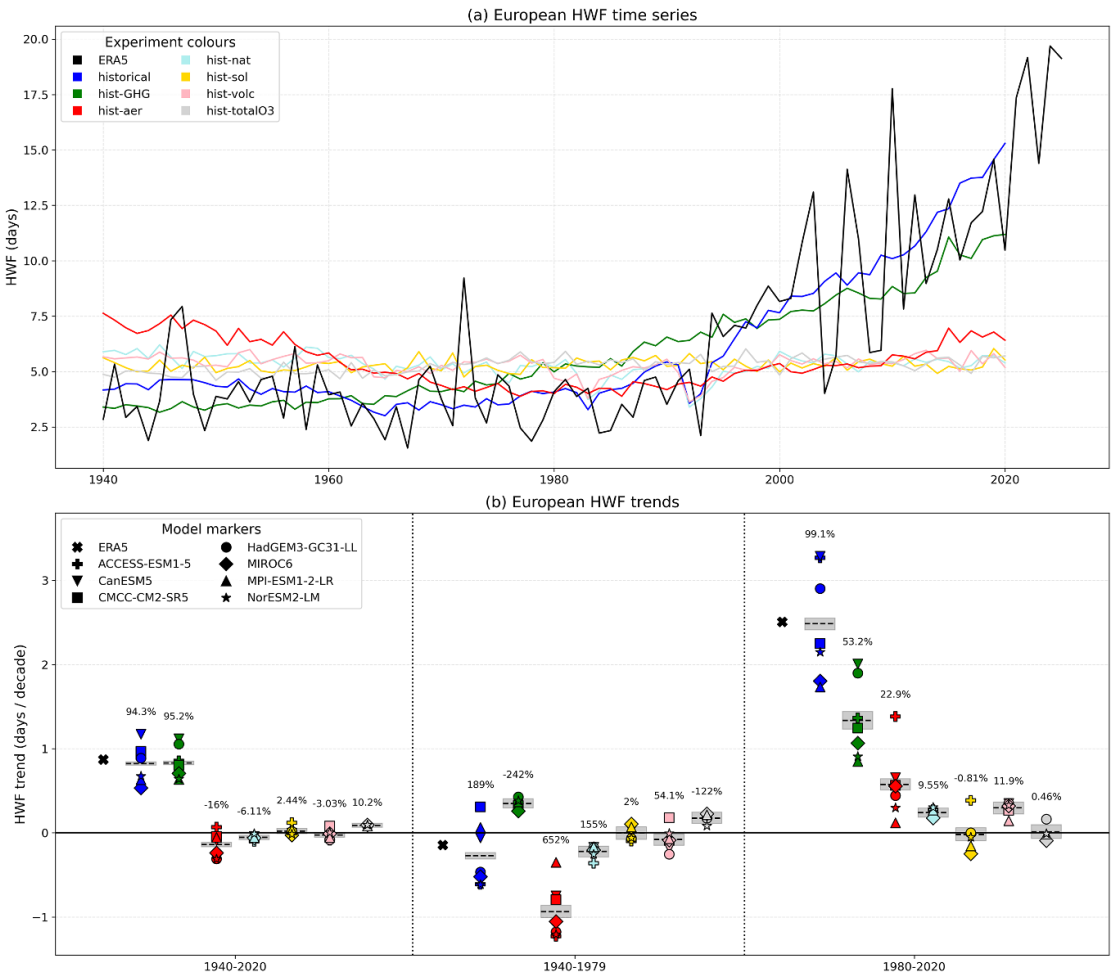

Figure 2. Comparison of ERA5 with LESFMIP models for HWF spatially averaged over the land area of Europe. (a) HWF for ERA5 and MMMs of HWF for all and single forcing experiments. (b) Theil–Sen trends for three time periods (1940–2020, 1940–1979 and 1980–2020) with each model shown as a unique symbol. The MMMs are shown as dashed horizontal lines, with grey shading for the 95% confidence interval on the MMM calculated using bootstrapping. Percentage contributions for the MMM of all model experiments against ERA5 data are shown.

trend of GHG emissions and reduction in aerosols in Europe, identifying heatwave-related atmospheric circulation patterns is important to improve prediction and projections of European summer heatwaves.

3.3. Major atmospheric circulation patterns linked to European summer heatwaves

Atmospheric circulation plays an essential role in driving heatwaves and relevant feedback processes [10], including usually featuring a blocking high, more shortwave radiation, warm air advection and positive soil moisture feedback. Here, we use the SOM method to group the daily geopotential height anomaly field for European heatwave days (see section 2.4) into four atmospheric circulation patterns (figure 3; see section 2.6 for details). This provides a convenient and robust way to link specific atmospheric circulation patterns to European summer heatwaves. Focusing on the most significant heatwave days that have a Europe-wide impact also improves the chance of capturing common large-scale atmospheric circulation patterns. As the SOMs were trained separately in each model experiment, we match model-derived SOM patterns with ERA5-derived SOM patterns by computing and comparing spatial correlations between those SOM patterns, setting a threshold of 0.4 to ensure high similarity (see 2.6 and supplementary figure 5). Only five models are available for the SOM analysis.

Overall, the four atmospheric circulation patterns each have a dominant feature of a blocking-like anomaly located on the European continent. Their blocking-high-like anomaly differs in position and is linked to larger-scale atmospheric circulation. They are named as Scandinavian blocking (Node 1), Summer North Atlantic Oscillation (SNAO)-blocking (Node 2), Russian blocking (Node 3) and Eastern European blocking (Node 4). The blocking-like high anomaly can modulate the downward shortwave radiation, cause adiabatic warming, induce warm air advection and trigger positive land surface feedback [10]. The positive phase of SNAO shifts the storm track northward and can co-occur with a blocking-high over Western and Northern

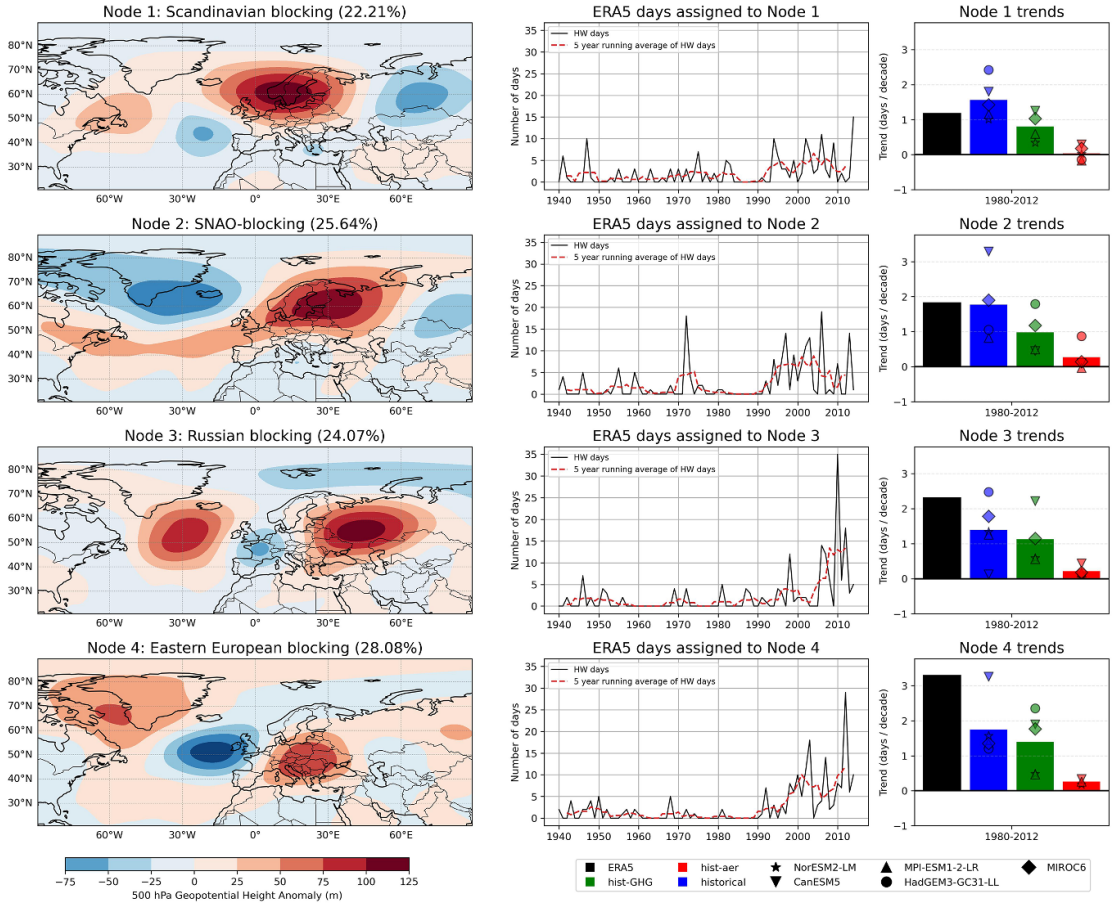

Figure 3. Atmospheric circulation patterns linked to European summer heatwaves derived from the SOM analysis. Only European heatwave days are included in the SOM analysis. (left) Geopotential height anomaly at 500 hPa (m) SOM patterns for ERA5 with headers giving the percentage of days assigned to that node; (centre) the number of days that are assigned to each SOM for each year (black) and the five-year running average (red) ; and (right) the Theil–Sen trends (days decade^{-1}) for ERA5, and all-forcings, hist-GHG and hist-aer MMMs for 1980–2012. The individual models are shown using unique markers.

Europe to induce heatwaves in these regions [63]. The Eastern European blocking pattern features a ridge over Southern Europe and North Africa, which facilitates hot air advection from North Africa. The Eastern European blocking (Node 4) is associated with the largest fraction of European heatwave days (28.08%), followed by SNAO-blocking (Node 2), Russian blocking (Node 3) and Scandinavian blocking (Node 1). The last two nodes also resemble a stationary Rossby wave pattern. The location of the blocking high anomaly largely determines the spatial impacts on heatwaves (supplementary figure 3). This is in agreement with the notion that atmospheric blocking and ridge lead to regionalised change in extremely hot days [64]. The number of days linked to these nodes has strong interannual variations, suggesting the complexity of European summer heatwave occurrence.

As the SOM analysis uses European heatwave days, and European heatwaves have become more frequent in recent decades (figure 1), many peaks associated with each nodes are also in recent decades. For example, the Russian blocking pattern is clearly linked to the intense 2010 Russian heatwave, which saw a strong and long-lived blocking event [65]. However, early heatwave events in clusters also relate to historical events, such as the 1972 Northern European heatwave [12] assigned to node 2, and the Central European heatwave of 1947 [66] split between nodes 1 and 4.

ERA5 trend analysis (black bars, right panels) shows that there is a larger trend in European heatwaves days associated with the Eastern European blocking pattern and the Russian blocking pattern than the other two circulation patterns. This is consistent with the larger HWF trends in Southern and Eastern Europe during the period 1980–2020. The MMM with historical forcing (blue bars) gives smaller trends for the last three nodes but a larger trend for the first node compared to ERA5. The Eastern European blocking pattern has the largest trend among all the nodes, confirming the larger HWF trend in Southern and Eastern Europe. These MMM trends are dominated by the GHGs forcing (green bars), in particular for the last two atmospheric circulation patterns. This

aligns with the dominant role of GHGs in driving the upward HWF trends in Europe in recent decades.

The four atmospheric circulation regimes identified in the SOM analysis are clearly linked to European summer heatwaves. However, as the trends discussed above only include those days with the most expansive heatwave activity, it is unclear whether the occurrence of the circulation pattern itself has changed, or whether trends mirror those found in European heatwave days. Therefore, to address trends in the circulation patterns themselves, and what role they may play in European HWF trends in recent decades, in figure 4 we compare all JJA days to these four nodes. To do this, we project daily geopotential height fields for all JJA days from both ERA5 and the model simulations onto the four atmospheric circulation patterns from figure 3 and assign each JJA day to a particular node if they have a spatial correlation of greater than 0.4 (see section 2.7 for more details). This allows us to determine whether any of the four circulation patterns have increased in occurrence in recent years, and assess whether the models capture circulation trends shown in ERA5. While both figure 4 and the third column of figure 3 show trends in the circulation patterns, figure 3 only includes European heatwave days, whereas figure 4 includes all summer days.

For ERA5, the Eastern European blocking pattern exhibits a large positive trend of around 2.6 days per decade (a positive trend in a similar circulation pattern was also found in [67, 68]) and the SNAO-blocking has a positive trend of around 1 day per decade. The trends for the other two circulation patterns are relatively small (as with a similar circulation pattern found in [69] over Scandinavia). This may imply that changes in circulation pattern occurrences have driven part of the positive HWF trends associated with the Eastern European blocking and SNAO-blocking patterns.

The MMM trends with historical and with individual forcings from the model simulations show that the large trend in the SNAO-blocking and Eastern European blocking patterns are not externally forced. For both patterns, the ERA5 value is within the ensemble spread of the models, suggesting a role of internal variability. However, for the Eastern European blocking pattern, there is only one ensemble member from the NorESM2-LM with historical forcing matching the ERA5 trend magnitude. No other ensemble members have such a large trend value. For the NorESM2-LM model, the experiments with GHGs and aerosols have half of the ensemble size as in that with historical forcing; this may explain why the ensemble spread is narrower for these two experiments. It is likely that the trend in Eastern European blocking is mainly internally driven but is underrepresented in most of the models examined in this study.

Climate models have been found to underestimate trends in atmospheric circulation, contributing to weaker trend in heat extremes in Western Europe [16, 23]. Here with large ensembles, we argue that the ERA5 trend in the Eastern European blocking pattern is more likely due to internal variability underestimated by most of the models. As the Eastern European blocking pattern is the most relevant for heatwaves in Southern and Eastern Europe (supplementary figure 3), it also helps to explain the less strong HWF trend in these regions in the all-forcings historical MMM compared to ERA5 (figure 1). This is further confirmed by examining the spatial distributions of the percentage contribution of historical forcing, GHGs and aerosols against the ERA5 data, The spatial pattern of percentage contribution suggests a relatively smaller contribution to ERA5 heatwave trends in Southern and particularly Eastern Europe by external forcings compared to other regions (supplementary figure 6). However, as the historical MMM captures the ERA5 Europe-averaged HWF trends well (figure 2), while not showing comparable circulation trends, this suggests that the models may have overestimated thermodynamic effects for Europe-averaged heatwave trends. GHGs and aerosols are not shown to have driven the frequency of the atmospheric circulation regimes to drive the recent European HWF trends. Instead, they have mainly impacted thermodynamic processes to increase the European HWF in the models. Therefore, the thermodynamic effects on recent European heatwave trends are likely overestimated in the models.

4. Summary and discussion

Using seven coupled climate models participating in the LESFMIP project, ERA5 reanalysis, and the SOM method, our analysis shows that GHGs are the major driver of the recent surge in HWF in Europe after 1980 with the reduction in aerosol emissions further amplifying it. GHGs and aerosols have respectively contributed to around 53% and 23% of the recent European heatwave trends. The historical forcing experiment reproduces a comparable trend compared to ERA5 for the periods 1940–2020 and 1980–2020. Aerosols have driven a notable negative trend in HWF in the earlier period, 1940–1979, with both GHGs and O3 driving a small positive trend. We note that there may be some nonlinear interactions between the different forcings, for example between GHGs and aerosols, in driving trends in HWF in Europe. This is because the linear addition of all individual forcings experiments results in a lower trend than the historical full-forcings experiment (figure 2). If GHGs continue to increase without considerable mitigation measures, this, coupled with the reductions in aerosols due to clean air policies, will likely drastically increase the HWF even further in Europe in the future. This will subsequently increase the risk to our societies, human health and infrastructure.

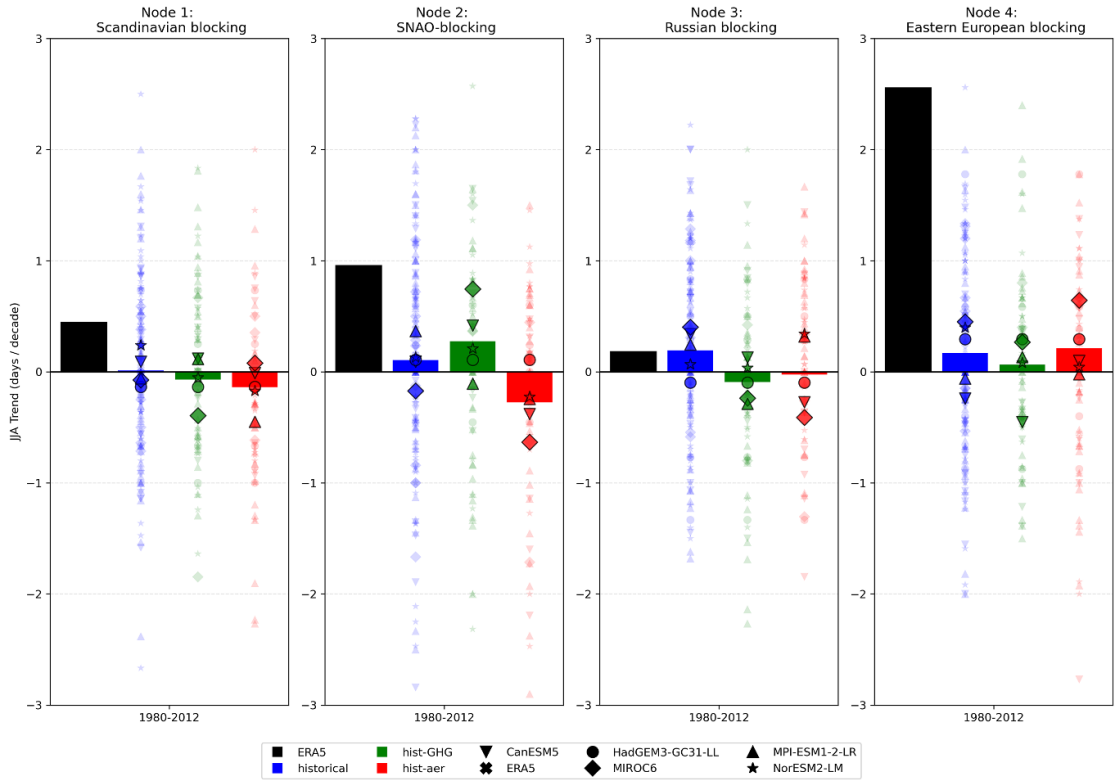

Figure 4. Theil–Sen trends (days decade^{-1}) in the occurrence (days per summer, JJA) of atmospheric circulation patterns projected onto the SOM nodes in figure 3 for ERA5 (black bars), and the LESFMIP MMMs for experiments all-forcings (blue bars), hist-GHG (green bars) and hist-aer (red bars) during the period 1980–2012. The individual model ensemble means are shown using unique markers and ensemble members shown with smaller, paler markers.

We use the SOM method to characterise the atmospheric circulation patterns that are linked to the most significant heatwave days in Europe in terms of spatial extent. The four identified atmospheric circulation regimes are dominated by a high-pressure anomaly located on the European continent. They are uniquely tied to heatwaves in different regions in Europe. These are in large part consistent with the existing understanding of atmospheric circulation patterns linked to European summer heatwaves. The Eastern European blocking circulation pattern has shown a large increasing trend after 1980 in ERA5 data. However, only one ensemble member from one model has captured this trend while the MMM trend is small. It is thus likely that the increase in the frequency of this atmospheric circulation regime is due to internal climate variability but is underrepresented in most of the models in this study. This internally-driven circulation trend does explain the underestimated HWF trend in Southern and Eastern Europe in the period after 1980 (figure 1). On the other hand, the trend in the Europe-averaged HWF in ERA5 is well captured by MMM in the historical all-forcings experiment. We do note, however, that the models show a range of trend values, suggesting varied sensitivity to radiative forcings. The direct thermodynamic impacts on HWF trends over Europe in the models may be overestimated. In this regard, improving model representation of these atmospheric circulation trends, and constraining model sensitivity to radiative forcings, are important for accurately attributing historical HWF trends and for predicting future HWF changes. This also highlights the complexity of the drivers of regional summer heatwaves within the European continent, and regional analysis/attribution is necessary to provide a more detailed understanding of European summer heatwaves. Future work on land surface feedback impacts and nonlinear interactions between different external forcing agents is also necessary to advance our understanding of European summer heatwave change.

Heat-related mortality in Europe due to heatwaves had been increasing between 1990 and 2004 [70] and is a major societal and health crisis [71]. Heatwaves are the most significant high-impact extreme events considering their attributable counts of death according to World Health Organisation and the European Environment Agency. Our attribution analysis has pointed to the substantial role of GHGs in driving the surge in European heatwaves after 1980, boosted by the reduction in aerosols. Internal climate variability likely has further amplified the increase in HWF and thus worsened the impacts in heatwave hotspots of Southern and Eastern Europe in terms of heat-related mortality rate

[70]. With significant mitigation measures to limit the increase in GHG emissions, negative impacts on mortality in Europe would have been reduced and some of the heat-related mortality may have been avoided. However, it is clear that future heat-related mortality can be reduced and partly prevented through bold mitigation policies in GHG emissions and health-risk assessment [72]. Better warning systems, including improved heatwave predictions and preventive actions, are also important.

Acknowledgments

KY was supported by the UKRI Horizon Europe Guarantee MSCA Postdoctoral Fellowship EP/Y029119/1, and by the John Fell Fund financed by Oxford University Press (Project Reference: 0013106). SO was supported by the NERC CANARI Programme and received funding from the European Union's Horizon 2020 research and innovation programme under grant agreement No 101003469 (XAIDA). TH was supported by the Rupert Ford Award, administered by the Royal Meteorological Society, in order to attend the EPESC-LEADER Science Meeting in Busan, South Korea, where the work for this paper was presented and discussed. This work used JASMIN, a facility provided by the UK's Centre for Environmental Data Analysis (https://www.jasmin.ac.uk; [73]).

Data availability statement

All analyses have been conducted using the ERA5 reanalysis (processed from https://climate.copernicus.eu) and LESFMIP model simulations (available from ESGF nodes https://esgf.github.io/nodes.html; https://ns9039k.web.sigma2.no/datapeak/LESFMIP/readme.txt (for NorESM2-LM); https://dapds00.nci.org.au/thredds/catalog/fs38/publications/CMIP6/DAMIP/CSIRO/ACCESS-ESM1-5/catalog.html (for ACCESS-ESM1-5)).

The data that support the findings of this study are openly available at the following URL/DOI: https://esgf-ui.ceda.ac.uk/search [74].

Supplementary Figures available at https://doi.org/10.1088/1748-9326/ae6d18/data1.

Competing interests

The authors declare no competing interests.

Materials & correspondence

Correspondence and material requests should be addressed to Kunhui Ye.

ORCID iDs

Tilda Huntingford 0009-0003-9197-8281
Kunhui Ye 0000-0002-9433-8066
Scott Osprey 0000-0002-8751-1211

References

[1] Ebi K L *et al* 2021 Hot weather and heat extremes: health risks *Lancet* **398** 698–708
[2] Matthews T, Raymond C, Foster J, Baldwin J W, Ivanovich C, Kong Q, Kinney P and Horton R M 2025 Mortality impacts of the most extreme heat events *Nat. Rev. Earth Environ.* **6** 193–210
[3] Brás T A, Seixas J, Carvalhais N and Jägermeyr J 2021 Severity of drought and heatwave crop losses tripled over the last five decades in Europe *Environ. Res. Lett.* **16** 065012
[4] Xu H, Xiao J and Zhang Z 2020 Heatwave effects on gross primary production of northern mid-latitude ecosystems *Environ. Res. Lett.* **15** 074027
[5] Stone B, Mallen E, Rajput M, Gronlund C J, Broadbent A M, Krayenhoff E S, Augenbroe G, O'Neill M S and Georgescu M 2021 Compound climate and infrastructure events: how electrical grid failure alters heat wave risk *Environ. Sci. Technol.* **55** 6957–64
[6] Robine J-M, Cheung S L K, Roy S L, Van Oyen H, Griffiths C, Michel J-P and Richard Herrmann F 2008 Death toll exceeded 70,000 in Europe during the summer of 2003 *Comptes Rendus. Biol.* **331** 171–8
[7] Ballester J, Quijal-Zamorano M, Fernando Méndez Turrubiates R, Pegenaute F, Herrmann F R, Robine J M, Basagaña X, Tonne C, Antó J M and Achebak H 2023 Heat-related mortality in Europe during the summer of 2022 *Nat. Med.* **29** 1857–66
[8] Barriopedro D, García-Herrera R, Ordóñez C, Miralles D G and Salcedo-Sanz S 2023 Heat waves: physical understanding and scientific challenges *Rev. Geophys.* **61** e2022RG000780
[9] Merz B *et al* 2020 Impact forecasting to support emergency management of natural hazards *Rev. Geophys.* **58** e2020RG000704
[10] Domeisen D I V, Eltahir E A B, Fischer E M, Knutti R, Perkins-Kirkpatrick S E, Schär C, Seneviratne S I, Weisheimer A and Wernli H 2023 Prediction and projection of heatwaves *Nat. Rev. Earth Environ.* **4** 36–50
[11] Pörtner H O et al. 2022 Climate change 2022: impacts, adaptation and vulnerability *Technical Report* (IPCC)
[12] Russo S, Sillmann J and Fischer E M 2015 Top ten European heatwaves since 1950 and their occurrence in the coming decades *Environ. Res. Lett.* **10** 124003
[13] Christidis N, Jones G S and Stott P A 2015 Dramatically increasing chance of extremely hot summers since the 2003 European heatwave *Nat. Clim. Change* **5** 46–50
[14] Fischer E M and Schär C 2010 Consistent geographical patterns of changes in high-impact European heatwaves *Nat. Geosci.* **3** 398–403

[15] Meehl G A and Tebaldi C 2004 More intense, more frequent and longer lasting heat waves in the 21st century *Science* **305** 994–7
[16] Vautard R *et al* 2023 Heat extremes in Western Europe increasing faster than simulated due to atmospheric circulation trends *Nat. Commun.* **14** 6803
[17] Stegehuis A I, Vogel M M, Vautard R, Ciais P, Teuling A J and Seneviratne S I 2021 Early summer soil moisture contribution to Western European summer warming *J. Geophys. Res.: Atmos.* **126** e2021JD034646
[18] Sousa P M, Barriopedro D, García-Herrera R, Ordóñez C, Soares P M M and Trigo R M 2020 Distinct influences of large-scale circulation and regional feedbacks in two exceptional 2019 European heatwaves *Commun. Earth Environ.* **1** 48
[19] Fischer E M, Seneviratne S I, Lüthi D and Schär C 2007 Contribution of land-atmosphere coupling to recent European summer heat waves *Geophys. Res. Lett.* **34** L06707
[20] Lee M-H, Lee S, Song H-J and Chang-Hoi H 2017 The recent increase in the occurrence of a boreal summer teleconnection and its relationship with temperature extremes *J. Clim.* **30** 7493–504
[21] Teng H and Branstator G 2019 Amplification of waveguide teleconnections in the boreal summer *Curr. Clim. Change Rep.* **5** 421–32
[22] Coumou D, Lehmann J and Beckmann J 2015 The weakening summer circulation in the Northern Hemisphere midlatitudes *Science* **348** 324–7
[23] Boé J *et al* 2020 Past long-term summer warming over western Europe in new generation climate models: role of large-scale atmospheric circulation *Environ. Res. Lett.* **15** 084038
[24] Dirmeyer P A, Mantripragada R S S, Gay B A and Klein D K D 2022 Evolution of land surface feedbacks on extreme heat: adapting existing coupling metrics to a changing climate *Front. Environ. Sci.* **10** 949250
[25] Stott P A, Stone D'ı A and Allen M R 2004 Human contribution to the European heatwave of 2003 *Nature* **432** 610–4
[26] Feser F, van Garderen L and Hansen F 2024 The summer heatwave 2022 over western Europe: an attribution to anthropogenic climate change *Bull. Am. Meteorol. Soc.* **105** E2175–9
[27] Yin Z, Dong B, Wei W and Yang S 2024 Anthropogenic impacts on amplified midlatitude European summer warming and rapid increase of heatwaves in recent decades *Geophys. Res. Lett.* **51** e2024GL108982
[28] Smith S J and Bond T C 2014 Two hundred fifty years of aerosols and climate: the end of the age of aerosols *Atmos. Chem. Phys.* **14** 537–49
[29] Hodnebrog Ø *et al* 2024 Recent reductions in aerosol emissions have increased Earth's energy imbalance *Commun. Earth Environ.* **5** 166
[30] Bauer S E, Tsigaridis K, Faluvegi G, Nazarenko L, Miller R L, Kelley M and Schmidt G 2022 The turning point of the aerosol era *J. Adv. Model. Earth Syst.* **14** e2022MS003070
[31] Wang P, Yang Y, Xue D, Ren L, Jianping Tang L R L and Liao H 2023 Aerosols overtake greenhouse gases causing a warmer climate and more weather extremes toward carbon neutrality *Nat. Commun.* **14** 7257
[32] Shi J-R, Wijffels S E, Kwon Y-O, Talley L D and Gille S T 2023 The competition between anthropogenic aerosol and greenhouse gas climate forcing is revealed by North Pacific water-mass changes *Sci. Adv.* **9** eadh7746
[33] Schumacher D L, Singh J, Hauser M, Fischer E M, Wild M and Seneviratne S I 2024 Exacerbated summer European warming not captured by climate models neglecting long-term aerosol changes *Commun. Earth Environ.* **5** 182
[34] Smith D *et al* 2022 Attribution of multi-annual to decadal changes in the climate system: the Large Ensemble Single Forcing Model Intercomparison Project (LESFMIP) *Front. Clim.* **4** 955414
[35] Luo B, Luo D, Zhuo W, Xiao C, Dai A, Simmonds I, Yao Y, Diao Y and Gong T 2023 Increased summer European heatwaves in recent decades: contributions from greenhouse gases-induced warming and Atlantic multidecadal oscillation-like variations *Earth's Future* **11** e2023EF003701
[36] Seong M-G, Min S-K, Kim Y-H, Zhang X and Sun Y 2021 Anthropogenic greenhouse gas and aerosol contributions to extreme temperature changes during 1951–2015 *J. Clim.* **34** 857–70
[37] Hersbach H *et al* 2020 TheERA5 global reanalysis *Q. J. R. Meteorol. Soc.* **146** 1999–2049
[38] Velikou K, Lazoglou G, Tolika K and Anagnostopoulou C 2022 Reliability of the ERA5 in replicating mean and extreme temperatures across Europe *Water* **14** 543
[39] Sheridan S C, Lee C C and Smith E T 2020 A comparison between station observations and reanalysis data in the identification of extreme temperature events *Geophys. Res. Lett.* **47** e2020GL088120
[40] Masson-Delmotte V *et al* 2021 Climate change 2021: the physical science basis *Contribution of Working Group I to the 6th Assessment Report of the Intergovernmental Panel on Climate Change* vol 2 p 2391
[41] Ziehn T, Chamberlain M A, Law R M, Lenton A, Bodman R W, Dix M, Stevens L, Wang Y-P and Srbinovsky J 2020 The Australian earth system model: ACCESS-ESM1.5 *J. South. Hemisph. Earth Syst. Sci.* **70** 193–214
[42] Swart N C *et al* 2019 The Canadian earth system model version 5 (CANESM5. 0.3) *Geosci. Model Dev.* **12** 4823–73
[43] Cherchi A *et al* 2019 Global mean climate and main patterns of variability in the CMCC-CM2 coupled model *J. Adv. Model. Earth Syst.* **11** 185–209
[44] Andrews M B *et al* 2020 Historical simulations with HADGEM3-GC3. 1 for CMIP6 *J. Adv. Model. Earth Syst.* **12** e2019MS001995
[45] Tatebe H *et al* 2019 Description and basic evaluation of simulated mean state, internal variability and climate sensitivity in MIROC6 *Geosci. Model Dev.* **12** 2727–65
[46] Müller W A *et al* 2018 A higher-resolution version of the Max Planck Institute earth system model (MPI-ESM1. 2-HR) *J. Adv. Model. Earth Syst.* **10** 1383–413
[47] Seland Ø *et al* 2020 Overview of the Norwegian Earth System Model (NorESM2) and key climate response of CMIP6 DECK, historical, and scenario simulations *Geosci. Model Dev. Discuss.* **13** 6165–200
[48] Gillett N P, Shiogama H, Funke B, Hegerl G, Knutti R, Matthes K, Santer B D, Stone D and Tebaldi C 2016 The detection and attribution model intercomparison project (DAMIP v1. 0) contribution to CMIP6 *Geosci. Model Dev.* **9** 3685–97
[49] Perkins S E and Alexander L V 2013 On the measurement of heat waves *J. Clim.* **26** 4500–17
[50] Zhang X, Hegerl G, Zwiers F W and Kenyon J 2005 Avoiding inhomogeneity in percentile-based indices of temperature extremes *J. Clim.* **18** 1641–51
[51] Gibson P B, Perkins-Kirkpatrick S E, Uotila P, Pepler A S and Alexander L V 2017 On the use of self-organizing maps for studying climate extremes *J. Geophys. Res.: Atmos.* **122** 3891–903
[52] Rousi E, Kornhuber K, Beobide-Arsuaga G, Luo F and Coumou D 2022 Accelerated western European heatwave trends linked to more-persistent double jets over Eurasia *Nat. Commun.* **13** 3851
[53] Johnson N C, Feldstein S B and Tremblay B 2008 The continuum of Northern Hemisphere teleconnection patterns and a description of the NAO shift with the use of self-organizing maps *J. Clim.* **21** 6354–71
[54] Lee S and Feldstein S B 2013 Detecting ozone-and greenhouse gas–driven wind trends with observational data *Science* **339** 563–7
[55] Lorenz R, Stalhandske Z and Fischer E M 2019 Detection of a climate change signal in extreme heat, heat stress and cold in Europe from observations *Geophys. Res. Lett.* **46** 8363–74
[56] Barriopedro D, Fischer E M, Luterbacher J, Trigo R M and García-Herrera R 2011 The hot summer of 2010:

redrawing the temperature record map of Europe *Science* **332** 220–4
[57] Seneviratne S I *et al* 2021 Weather and climate extreme events in a changing climate *Climate Change 2021: The Physical Science Basis. Contribution of Working Group I to the Sixth Assessment Report of the Intergovernmental Panel on Climate Change* ed (Cambridge University Press) ch 11, pp 1513–766
[58] Mora C *et al* 2018 Broad threat to humanity from cumulative climate hazards intensified by greenhouse gas emissions *Nat. Clim. Change* **8** 1062–71
[59] Masselot P *et al* 2023 Excess mortality attributed to heat and cold: a health impact assessment study in 854 cities in Europe *Lancet Planet. Health* **7** e271–81
[60] Janoš T, Quijal-Zamorano M, Shartova N, Gallo E, Fernando Méndez Turrubiates R, Denisse Beltrán Barrón N, Peyrusse F and Ballester J 2025 Heat-related mortality in Europe during 2024 and health emergency forecasting to reduce preventable deaths *Nat. Med.* **31** 1–10
[61] Feichter J, Roeckner E, Lohmann U and Liepert B 2004 Nonlinear aspects of the climate response to greenhouse gas and aerosol forcing *J. Clim.* **17** 2384–98
[62] Schmidt A *et al* 2018 Volcanic radiative forcing from 1979 to 2015 *J. Geophys. Res.: Atmos.* **123** 12491–508
[63] Li M, Yao Y, Simmonds I, Luo D, Zhong L and Chen X 2020 Collaborative impact of the NAO and atmospheric blocking on European heatwaves, with a focus on the hot summer of 2018 *Environ. Res. Lett.* **15** 114003
[64] Sousa P M, Trigo R M, Barriopedro D, Soares P M M and Santos J ao A 2018 European temperature responses to blocking and ridge regional patterns *Clim. Dyn.* **50** 457–77
[65] Dole R, Hoerling M, Perlwitz J, Eischeid J, Pegion P, Zhang T, Quan X-W, Taiyi X and Murray D 2011 Was there a basis for anticipating the 2010 Russian heat wave? *Geophys. Res. Lett.* **38** 2011
[66] Harrington L J, Otto F E L, Cowan T and Hegerl G C 2019 Circulation analogues and uncertainty in the time-evolution of extreme event probabilities: evidence from the 1947 Central European heatwave *Clim. Dyn.* **53** 2229–47
[67] Horton D E, Johnson N C, Singh D, Swain D L, Rajaratnam B and Diffenbaugh N S 2015 Contribution of changes in atmospheric circulation patterns to extreme temperature trends *Nature* **522** 465–9
[68] Faranda D, Messori G, Jezequel A, Vrac M and Yiou P 2022 Atmospheric circulation compounds anthropogenic warming and extreme climate impacts in Europe *AGU Fall Meeting Abstracts* vol 2022 p A53G–06
[69] Iles C E, Vautard R and Vrac M 2025 No robust sign of human influence in the unprecedented atmospheric circulation of summer 2018 over Northern Europe *Earth's Future* **13** e2025EF006290
[70] D'Ippoliti D *et al* 2010 The impact of heat waves on mortality in 9 European cities: results from the EuroHEAT project *Environ. Health* **9** 37
[71] Kovats R S and Ebi K L 2006 Heatwaves and public health in Europe *Eur. J. Public Health* **16** 592–9
[72] Ignjačević P, Botzen W, Estrada F, Daanen H and Lupi V 2024 Climate-induced mortality projections in Europe: estimation and valuation of heat-related deaths *Int. J. Disaster Risk Reduct.* **111** 104692
[73] Lawrence B N, Bennett V L, Churchill J, Juckes M, Kershaw P, Pascoe S, Pepler S, Pritchard M and Stephens A 2013 Storing and manipulating environmental big data with JASMIN *2013 IEEE Int. Conf. on big Data* (IEEE) pp 68–75
[74] Available at: https://esgf-ui.ceda.ac.uk/search